

Defects in HgTe grown by molecular beam epitaxy on (211)B-oriented CdZnTe substrates

E. Selvig, C. R. Tonheim, K. O. Kongshaug, T. Skauli, T. Lorentzen, and R. Haakenaasen

Citation: *Journal of Vacuum Science & Technology B* **25**, 1776 (2007); doi: 10.1116/1.2787876

View online: <http://dx.doi.org/10.1116/1.2787876>

View Table of Contents: <http://scitation.aip.org/content/avs/journal/jvstb/25/6?ver=pdfcov>

Published by the AVS: Science & Technology of Materials, Interfaces, and Processing

Articles you may be interested in

II-VI heterostructures obtained by encapsulation of colloidal CdSe nanowires by molecular beam epitaxy deposition of ZnSe

J. Vac. Sci. Technol. B **29**, 03C102 (2011); 10.1116/1.3547715

Defects in CdHgTe grown by molecular beam epitaxy on (211)B-oriented CdZnTe substrates

J. Vac. Sci. Technol. B **26**, 525 (2008); 10.1116/1.2868782

Improve molecular beam epitaxy growth of HgCdTe on CdZnTe (211)B substrates using interfacial layers of Hg Te/Cd Te superlattices

J. Appl. Phys. **100**, 114316 (2006); 10.1063/1.2399890


Formation mechanism of crater defects on HgCdTe/CdZnTe (211) B epilayers grown by molecular beam epitaxy

Appl. Phys. Lett. **83**, 4785 (2003); 10.1063/1.1633017

Mercury cadmium telluride/tellurium intergrowths in HgCdTe epilayers grown by molecular-beam epitaxy

Appl. Phys. Lett. **82**, 2275 (2003); 10.1063/1.1566462


Instruments for Advanced Science

<p>Contact Hiden Analytical for further details: W www.HidenAnalytical.com E info@hiden.co.uk CLICK TO VIEW our product catalogue</p>	 <p>Gas Analysis</p> <ul style="list-style-type: none"> › dynamic measurement of reaction gas streams › catalysis and thermal analysis › molecular beam studies › dissolved species probes › fermentation, environmental and ecological studies 	 <p>Surface Science</p> <ul style="list-style-type: none"> › UHV TPD › SIMS › end point detection in ion beam etch › elemental imaging - surface mapping 	 <p>Plasma Diagnostics</p> <ul style="list-style-type: none"> › plasma source characterization › etch and deposition process reaction › kinetic studies › analysis of neutral and radical species 	 <p>Vacuum Analysis</p> <ul style="list-style-type: none"> › partial pressure measurement and control of process gases › reactive sputter process control › vacuum diagnostics › vacuum coating process monitoring
--	--	--	--	--

Defects in HgTe grown by molecular beam epitaxy on (211)B-oriented CdZnTe substrates

E. Selvig,^{a)} C. R. Tonheim, K. O. Kongshaug, T. Skauli, T. Lorentzen, and R. Haakenaasen
Norwegian Defence Research Establishment, P.O. Box 25, N-2027 Kjeller, Norway

(Received 11 May 2007; accepted 28 August 2007; published 12 October 2007)

The authors present a systematic study showing the evolution of the defect morphology and crystalline quality in molecular beam epitaxially grown HgTe epilayers with substrate temperature. The authors have characterized the layers using optical microscopy, atomic force microscopy, scanning electron microscopy, energy dispersive x-ray spectroscopy, and high-resolution x-ray diffraction. Four types of defects (microvoids, circular voids, hillocks, and high-temperature voids) have been characterized on epilayers grown in the substrate temperature range of 183.3–201.3 °C. The authors find that there is a minimum in the area covered by defects at a temperature just below the onset of Te precipitation, and they define this temperature as the optimal growth temperature. Above the optimal growth temperature the authors observe the appearance of high-temperature voids. By determining the onset of Te precipitation in HgTe, and performing thermodynamic calculations, the authors can also successfully predict the onset of Te precipitation in CdHgTe, which again is related to the optimal growth temperature in CdHgTe. Furthermore, the authors have found that the shape and density of the microvoids are particularly sensitive to the substrate temperature, and that these properties can be used to determine the deviation from the optimal growth temperature. From the shape and density of microvoids in one growth of HgTe, the authors can therefore determine the temperature correction needed to reach the optimal growth temperature for CdHgTe. The authors also suggest a mechanism for the formation of the microvoids based on the assumption of impurities on the substrate combined with a preferential Te diffusion in the $[\bar{1}11]$ direction across the steps. © 2007 American Vacuum Society. [DOI: 10.1116/1.2787876]

I. INTRODUCTION

CdHgTe is an important material for infrared detectors^{1,2} as the direct band gap can be compositionally tuned from –0.26 to 1.61 eV at 77 K.³ Defects in CdHgTe can be detrimental to detector performance,^{4,5} and it is therefore important to optimize the growth conditions to reduce their density. It has previously been shown, using reflection high-energy electron diffraction (RHEED), that pure 2D growth of CdHgTe on CdZnTe (211)B by molecular beam epitaxy (MBE) is obtained at temperatures below the onset of Te precipitation.⁶ The temperature where the latter occurs depends on the Hg flux, and it has previously been shown that this dependence is consistent with thermodynamical predictions of the Te-rich side of the CdHgTe phase diagram.^{7,8} Hence, the substrate temperature at the onset of Te precipitation is termed the Te-phase limit, and above this temperature Te precipitation (due to a too high Hg re-evaporation rate) develops into large defects which are often detrimental to photodiodes, as shown by current-voltage measurements or that the defects may extend all the way down to the substrate-layer interface.^{4,9–13} In the literature these defects have been called V-shaped defects,¹⁴ surface crater voids,¹⁰ and voids.^{13,15,16} We here call these defects high-temperature voids. At low substrate temperatures so-called microvoids are formed and twinning occurs.^{6,9,10}

The optimal temperature for CdHgTe growth, T_{opt} , is found to be just below the Te-phase limit. Other groups have also shown that at this temperature a low dislocation density is combined with a good surface morphology.^{9,17} A deviation in the growth temperature of a few degrees from T_{opt} significantly changes the surface defect density.

Defect studies in the CdHgTe material system have been performed by He *et al.*, who describe several types of defects and their relation to substrate preparation and growth conditions.⁹ Aoki *et al.* performed transmission electron microscopy (TEM) and found that high-temperature voids contain grains of CdHgTe surrounded by elemental Te.¹¹ Almeida *et al.* reported surface defect densities, etch pit densities, and x-ray diffraction (XRD) full width at half maximum (FWHM) on CdHgTe layers grown at different temperatures and on different substrate orientations.¹⁷ Piquette *et al.* have minimized high-temperature voids and microdefects by selecting substrates of high quality and with low Te precipitate content and optimizing growth rates.¹⁵

We present a systematic study of defect shape and density versus substrate temperature in HgTe epilayers grown on CdZnTe (211)B substrates. HgTe is a simpler material system than CdHgTe, with fewer process parameters, but presents very similar challenges as CdHgTe with respect to crystalline quality. Thus, the results obtained here can help us understand defect formation in the more complicated CdHgTe material. Furthermore, we find sharper defect features in HgTe than in CdHgTe, which suggests a lower sur-

^{a)}Electronic mail: espen.selvig@ffi.no

face mobility for Cd than Te (i.e., Cd sticks closer to where it lands, whereas Hg easily re-evaporates from the surface and Te diffuses much farther).

Included in the study are microvoids, circular voids, hillocks, and high-temperature voids. We have found that both the shape and the density, especially of the microvoids, vary significantly for small changes in the substrate temperature, and that the minimum area covered by defects is obtained just below the Te-phase limit, which coincides with T_{opt} as it is defined by other groups for CdHgTe. Of particular interest is the shape of the microvoids, which consist of a set of very planar surfaces. We show how the distinct shape of these can be used to determine the deviation from the optimal growth temperature. Using a thermodynamic model we show that the Te-phase limit in HgTe can be used to predict the Te-phase limit in CdHgTe. Hence, the optimal growth temperature for CdHgTe can be found from the shape of the microvoids in just one grown HgTe layer.

We also present a model for the formation of the microvoids based on the assumption of impurities on the substrate combined with a preferential Te diffusion in the $[\bar{1}11]$ direction across the steps.

II. EXPERIMENTAL PROCEDURES

MBE growth of 3- μm -thick HgTe layers was performed on (211)B-oriented CdZnTe 7.5×7.5 mm substrates (wire-sawn from 15×15 mm substrates). The substrate orientation (211)B was chosen to reduce the twin content in the grown epilayer.^{6,18} The MBE machine was a 32P Riber machine equipped with a Riber MCL160 Hg source and a Te low-temperature SUMO source from Veeco. The substrate temperature was changed from sample to sample in increments of 1–2 °C over an 18 °C range. All other growth parameters were kept constant from sample to sample. The nominal growth rate was 500 Å/min. Growth rates were determined from grown CdHgTe layers that were measured by transmission spectroscopy. Small day-to-day variations in growth rate will not affect the result as the large Hg flux ($8.50 \cdot 10^{20} \text{ m}^{-2} \text{ s}^{-1}$) used can accommodate a large range of growth rates.

The heaters of the substrate and Hg source were turned off simultaneously so that the epilayers cooled down in a decreasing Hg flux. A similar series of CdHgTe samples was grown, with x -values 0.27–0.44. The detailed results of this will be published elsewhere, but information about the presence of high-temperature voids will be included in the section on thermodynamic model prediction of the Te-phase limit.

Polished 15×15 mm substrates were delivered by the supplier. These were wire-sawn into four 7.5×7.5 mm pieces. The polished side was laid down into melted wax (quartz sticky wax from South Bay Technologies) on a graphite holder. The substrate was then sawn using a slurry of boron carbide powder (800 grit), glycerine, and water. The substrate was removed from the graphite holder by gentle heating which melted the wax. Removal of wax residue was performed by immersing the sample for 2 min in each of the

following: boiling trichloroethylene, boiling acetone, and cold methanol. This cleaning procedure was performed twice.

The small substrates then underwent our standard substrate preparation process: blow with nitrogen, etch for 2 min in a 1% Br:methanol solution, rinse in methanol, blow dry in nitrogen, and mount on a molybdenum block using Ga. When mounted on the block there was a flow of nitrogen gas on the sample. The block was then quickly loaded into the MBE machine.

The substrate temperature was measured using a spring-loaded Ga-wetted thermocouple in contact with the back of the molybdenum block.¹⁹ Using this setup we could rotate the sample during growth and still obtain good thermal contact between the thermocouple and the substrate with a highly repeatable reading of the substrate temperature. To ensure that the temperature measurement system did not drift, In melting point (156.6 °C) measurements were performed prior to, during, and after growth of the series of layers described above. The maximum deviation between the measured In melting point temperatures was 1.1 °C, showing that there was little drift in the substrate temperature measurement system over this one-month period.

After growth the layers were inspected by optical microscopy, atomic force microscopy (AFM), scanning electron microscopy (SEM) with energy dispersive x-ray spectroscopy (EDX), and high-resolution x-ray diffraction (HRXRD). In HRXRD the 422 and 533 reflections, as well as the 533 twin reflection, were measured. The twin content was estimated by dividing the integrated intensity of the 533 twin reflection by the sum of the integrated intensities of the 533 reflection and the 533 twin reflection.

III. RESULTS AND DISCUSSION

A. HgTe surface morphology

We will in the following discuss the shape of the defects in the 11 HgTe layers grown in the temperature range 183.3–201.3 °C. We will show below that T_{opt} was found to be 193.3 °C. For simplicity we will give all temperatures in the discussion as a deviation in degrees Celsius from T_{opt} . Four main types of defects were observed in the HgTe layers: microvoids, circular voids, hillocks, and high-temperature voids.

Microvoids have also been called triangle defects in the literature.⁵ Microvoids are faceted, and their basic shape is an indented diamond with a longer axis in the step flow direction, $[1\bar{1}\bar{1}]$, and a shorter axis along the step direction, $[01\bar{1}]$, as shown in Fig. 1(e). The edges of the diamond are along the $[\bar{2}13]$, $[\bar{2}31]$, $[\bar{1}20]$, and $[\bar{1}02]$ directions. These edges are built up higher than the film surface outside the microvoid. The $[\bar{2}13]$, $[\bar{2}31]$, and $[01\bar{1}]$ directions are the intersections of the $\{111\}$ planes with the (211) surface and the directions along which cross-hatching occurs.²⁰ We have not, however, been able to identify the diamond facets as specific planes [they seem to have varying angles with the (211) surface]. At the center of the diamond there is a hole,

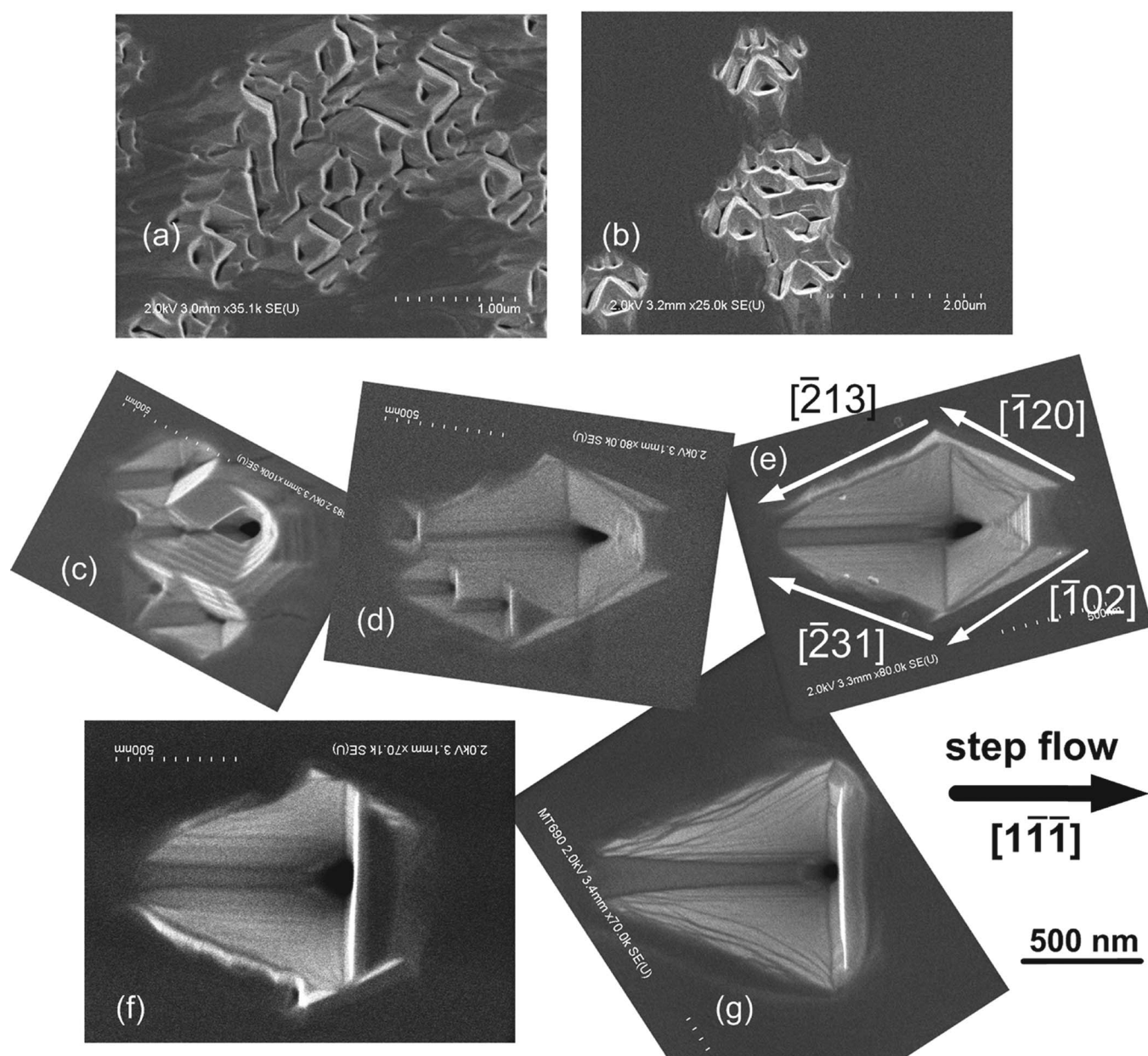


FIG. 1. SEM images of microvoids found in HgTe layers grown at different substrate temperatures (indicated): (a) Connecting superclusters ($T_{\text{opt}}-10$); (b) superclusters ($T_{\text{opt}}-6$); (c) cluster of diamond-shaped microvoids ($T_{\text{opt}}-4$); (d) Batlike-shaped with extra, small microvoids around the periphery ($T_{\text{opt}}-2$); (e) Batlike-shaped (T_{opt}); (f) almost triangular ($T_{\text{opt}}+1$); and (g) triangular ($T_{\text{opt}}+6$). Scale and orientation are equal for panels (c)–(g). The stepflow direction is indicated for panels (c)–(g).

and from this hole out along the long axis there is usually a “canal” extending all the way up to the film surface. The overall trend as the growth temperature is varied from low to high is that the microvoids develop from diamond shaped to triangular, and from clusters to single microvoids. At the lowest temperatures the microvoids form superclusters, and as the defects grow into each other the holes get distorted into lines or triangles with various planar walls between them, as shown in Figs. 1(a) and 1(b). At $T_{\text{opt}}-10$ the connected superclusters cover approximately 50% of the area, whereas at $T_{\text{opt}}-6$ they form smaller clusters (typically 5–9 microvoids) and cover less area. At $T_{\text{opt}}-4$ there are small

clusters (typically 2–5) of diamond-shaped microvoids, Fig. 1(c). Above this temperature the diamonds are gradually being cut off by an edge parallel to the short axis of the diamond [Figs. 1(d)–1(f)] until $T_{\text{opt}}+6$, where the diamond has become a triangle with a vertical ($\bar{1}11$) plane right next to the hole, Fig. 1(g). At $T_{\text{opt}}-2$ the microvoids are either single or have some smaller microvoids around their edges, Fig. 1(d). The diamond is slightly truncated, and the remaining facets extending above the film surface give the defect a “batlike” appearance. At the optimal growth temperature T_{opt} the microvoids are all single and of batlike shape, Fig. 1(e). At

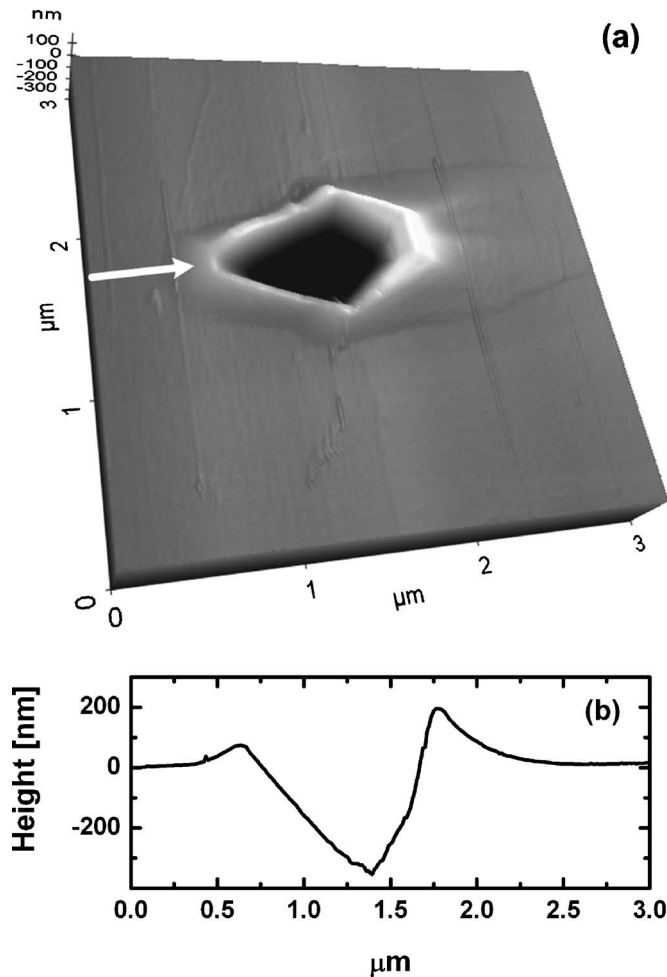


FIG. 2. (a) AFM image of a microvoid (T_{opt}); (b) height profile along direction indicated by the arrow. Arrow also points in the stepflow direction.

$T_{\text{opt}}+1$ there are both single batlike microvoids and microvoids with the vertical ($\bar{1}\bar{1}1$) cutoff plane closer to the hole, giving a shape closer to triangular, Fig. 1(f). These latter ones can have small microvoids around their periphery. At $T_{\text{opt}}+6$ the microvoids are single and triangular, Fig. 1(g). The vertical ($\bar{1}\bar{1}1$) plane now cuts through the middle of the hole at the bottom. At $T_{\text{opt}}+8$ there are very few microvoids, and the ones found looked like a much less developed version of the ones at $T_{\text{opt}}+6$ (i.e., they have the shape of beginning triangles).

The length of the microvoids increases from ~ 0.5 to $1.2 \mu\text{m}$ in the temperature range $T_{\text{opt}}-4$ to $T_{\text{opt}}+4$. An AFM image of a microvoid grown at T_{opt} is shown in Fig. 2. The measured depth is $\sim 0.4 \mu\text{m}$ (but the AFM tip does not get into the hole seen in the SEM images), whereas the parts of the facets surrounding the actual void form an elevation of $0.05\text{--}0.2 \mu\text{m}$ relative to the (211) surface. This elevation is significantly higher on the step-flow direction side of the defect (right side of the diamond in Figs. 1(e)), which we will call the upstream side (see Sec. III B), and it is $\sim 0.5 \mu\text{m}$ wide at T_{opt} . In addition to this facet elevation, there is a small buildup of material upstream out to

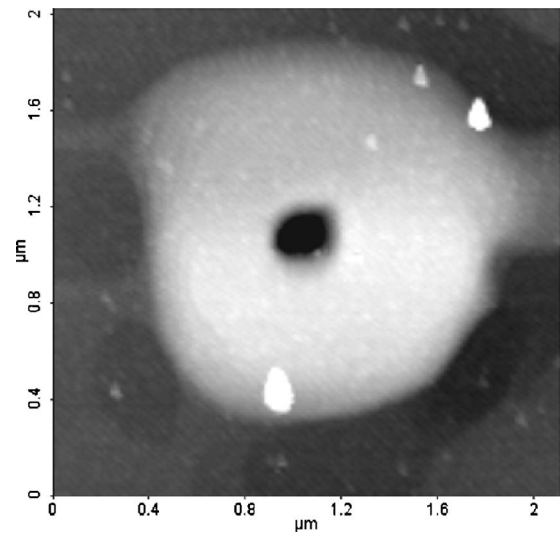


FIG. 3. AFM image of a circular void ($T_{\text{opt}}-2$).

$\sim 0.9 \mu\text{m}$ away from the void. At the highest temperatures there is no extra elevation on the upstream side.

EDX point spectra and line scans across microvoids in HgTe showed no difference between the composition in the microvoid and the surrounding layer. This is in agreement with the results of He *et al.* on microvoids in CdHgTe.⁹ Zhang and Summers showed the microvoid morphology in metalorganic molecular beam epitaxy grown CdHgTe, some of which are similar to that depicted in Fig. 1.¹⁶

A frequently observed defect in CdHgTe is the hillock defect.²¹ We have observed hillocks in the HgTe layers grown from $T_{\text{opt}}-2$ to $T_{\text{opt}}+6$. The hillocks have small height, vary in shape from almost circular to elongated, and can be difficult to distinguish from undulations on the surface. It is therefore difficult to determine the density of the hillocks. Another type of void looks circular, as shown in Fig. 3, with a diameter of $0.35\text{--}0.60 \mu\text{m}$ (increasing with temperature) and a depth of $5\text{--}30 \text{ nm}$. These voids were observed in layers grown at $T_{\text{opt}}-2$ and above, and we call them circular voids. Most of the circular voids were in the middle of what looks like hillocks ($4\text{--}10 \text{ nm}$ high), but the size of the hillocks decreases with temperature and only a small rim is left around the circular voids at the highest temperature.

At $T_{\text{opt}}+1$ another larger type of void appears, shown in Fig. 4. Because this type of void appears only above a certain temperature (for fixed Hg flux) we call this defect “high-temperature void.” The high-temperature voids are much wider and deeper than the microvoids, and their width increases rapidly with growth temperature. The width of the voids increases from 2 to $100 \mu\text{m}$, and the depth increases from 0.6 to $1.2 \mu\text{m}$ as the substrate temperature is increased from $T_{\text{opt}}+1$ to $T_{\text{opt}}+8$. There can be a small rim of built-up material around the void ($10\text{--}100 \text{ nm}$ high, 100 nm wide). High-temperature voids from layers grown at $T_{\text{opt}}+6$ and $T_{\text{opt}}+8$ are shown in Fig. 4.

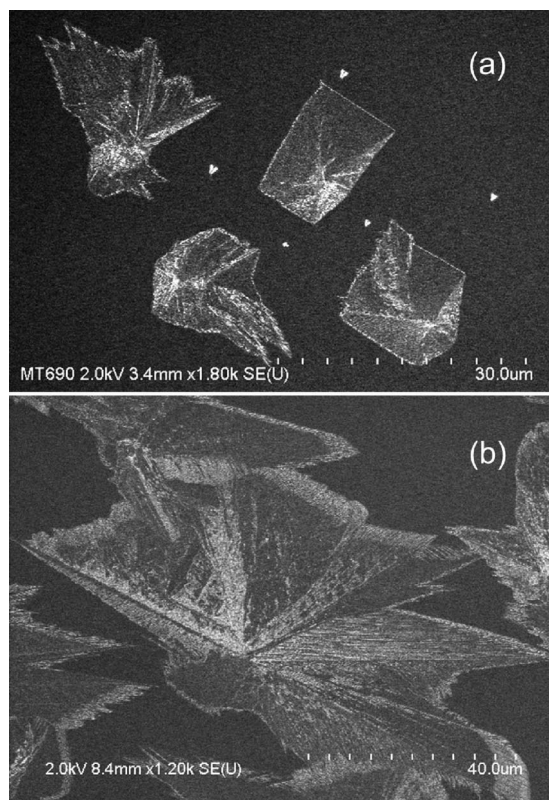


FIG. 4. SEM images of high-temperature voids in HgTe grown at (a) $T_{\text{opt}} + 6$ and (b) $T_{\text{opt}} + 8$. Smaller defects in (a) are triangular microvoids.

Many high-temperature voids have edges that look rather straight (straighter than in CdHgTe), and at higher substrate temperatures these voids become more and more star-shaped (Fig. 4). The high-temperature voids have relatively smooth walls, as opposed to the more polycrystalline look of high-temperature voids in CdHgTe. However, high-magnification SEM images of the near-surface region show that the interior walls of the voids are rough on a 100 nm scale and hence probably polycrystalline also in HgTe. EDX point spectra show that the voids contain Hg-deficient nonstoichiometric HgTe. EDX line scans across the high-temperature voids give a large decrease in Hg signal and a slight increase in Te signal inside the void, as shown in Fig. 5.

The density of the different defects in HgTe layers versus substrate temperature is shown in Fig. 6. Datapoints at a given temperature represent one sample. The samples were inspected in an optical microscope, and a representative area was found. Then, a picture with area $110 \times 80 \mu\text{m}$ was taken, and the defects were counted. On samples with lower defect density, several consecutive pictures were taken (up to nine), and pictures with smaller magnification ($430 \times 580 \mu\text{m}$) were taken to count the HT voids. The edges of the samples were avoided. There are clear trends as the temperature is varied. HgTe layers grown at a low substrate temperature contain a high density of microvoids which decreases rapidly with increasing temperature. At the two lowest temperatures the microvoids form more or less connected superclusters, and it is impossible to count individual

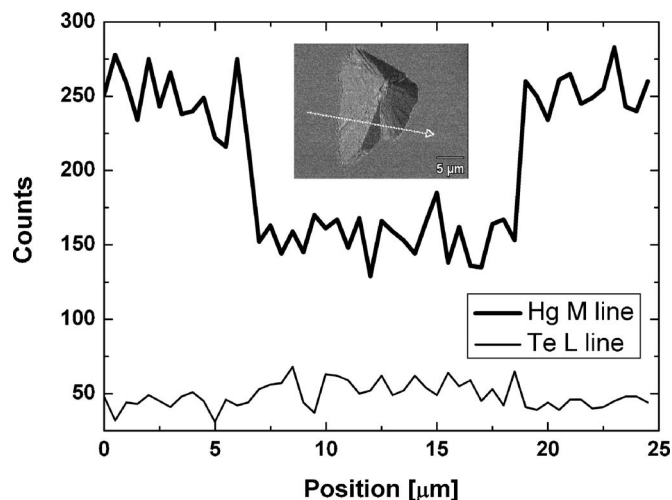


FIG. 5. Profiles of the Hg and Te EDX signals across a high-temperature void (inset).

microvoids. At $T_{\text{opt}} - 8$ and $T_{\text{opt}} - 6$ we have counted clusters of microvoids, which are plotted with a different symbol than the microvoids in the other samples. The number of individual microvoids is significantly higher. At $T_{\text{opt}} - 10$ it was not meaningful to count a number density; suffice it to say that the microvoid superclusters cover approximately 50% of the surface area. At the highest temperature, $T_{\text{opt}} + 8$, there were only occasional microvoids—too few to be counted meaningfully.

The density of the high-temperature voids that appear at 194.3°C does not vary much, but there is a slight increase with temperature to $T_{\text{opt}} + 6$ and then a drop at the highest temperature. As mentioned above, their widths increase fast

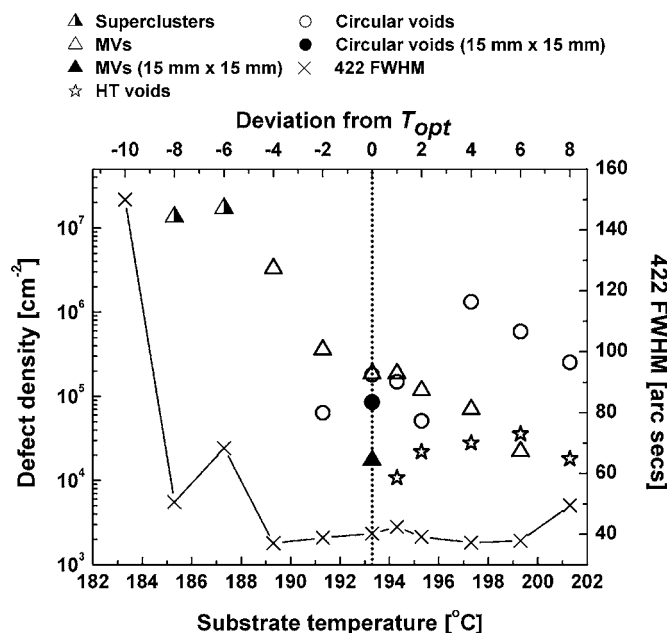


FIG. 6. Defect density and HRXRD 422 FWHM in HgTe layers plotted vs substrate temperature. 'MV's' = microvoids, 'HT voids' = high-temperature voids. Note that the symbols for MVs and circular voids overlap at T_{opt} .

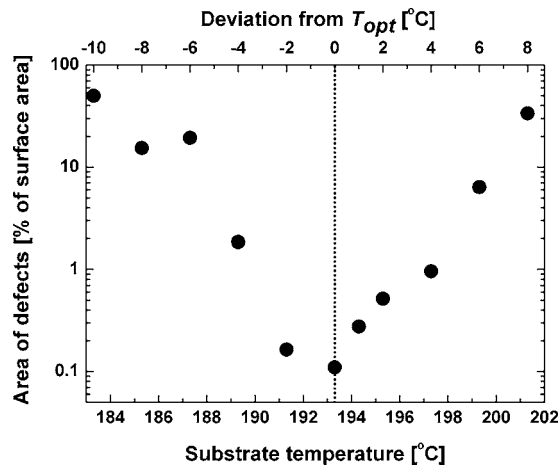


FIG. 7. Percent of the surface area covered by defects for the same layers as in Fig. 6.

with increasing substrate temperature. Almeida *et al.* also see an increase in high-temperature void density with temperature for CdHgTe layers on several substrate orientations.¹⁷ The decrease in number density at the highest temperature could be due to the separate high-temperature voids coalescing. These defects will be further discussed in the section on thermodynamic modeling. Hillock densities were not included due to the difficulty of distinguishing some of the hillocks from undulations on the surface. The density of circular voids shows no clear trend around T_{opt} , but it increases sharply at $T_{\text{opt}}+4$ in order to fall again above this temperature.

The optimal growth temperature with respect to surface area covered by defects is sharply defined as the temperature 1 °C below the onset of high-temperature voids, i.e., 193.3 °C, as shown in Fig. 7. At this temperature the microvoid density is low, whereas the larger high-temperature voids are absent. The area of microvoids, high-temperature voids, and the void part of circular voids (not the hillock around) has been included in the estimate. We get very similar curves, with minimum area at the same temperature, if we include the hillock area around the circular voids or exclude circular voids from the estimate.

The high microvoid defect density in the layers shown here is probably due to the substrates being sawed into four pieces prior to growth. The microvoid defect density on a HgTe layer grown at T_{opt} on a 15 × 15 mm substrate (not sawn) is also shown in Fig. 6 (filled triangle), and it is a factor of 11 lower than on the sample grown on a cut substrate. In a similar series of CdHgTe layers an even larger reduction in microvoid density, a factor 73, was found in CdHgTe grown on an uncut substrate relative sawed substrates (this will be published separately). We believe that either dust from the sawing or contamination from the wax or dissolving-cleaning agents used in the sawing process acts as potential nucleation centers for microvoids. Other groups have also reduced the sample defect density by careful substrate selection¹⁵ or substrate preparation.⁹ Given the highly varying microvoid density seen in Fig. 6 (more than two

orders of magnitude), the actual nucleation of microvoids clearly depends on the growth conditions as well as on substrate preparation. We have no reason to believe that the temperature variation of the defect densities should look dramatically different in samples with a different substrate preparation.

B. Mechanism for formation of microvoids

Figure 1(e) contains all the qualitative features seen in the microvoids. An impurity on the surface (or substrate defect) could block diffusion of atoms so that material would gather around it. Let us assume that there is no or less growth on impurities, as indicated by the holes we see in the middle of all the microvoids. We suggested earlier, as part of a theory for formation of needle structures in CdHgTe, that the Te atoms in CdHgTe diffuse preferentially in the $[\bar{1}11]$ direction across the steps, whereas they have no preferential diffusion direction on the symmetric (111) surface.²² Let us assume also for HgTe that the Te atoms diffuse preferentially in the $[\bar{1}11]$ direction (that is, opposite to the step-flow direction), whereas there is no preferential diffusion on any symmetric planar surface. Then, if diffusion is blocked by an impurity, material must build up on the upstream side of the hole [right side of the hole in Fig. 1(e)], while there should be a deficiency of material on the downstream side of the hole [left side of the hole in Fig. 1(e)]. This is indeed what we see in AFM profiles of the diamond-shaped microvoids; material has built up on the upstream side while the most of the depression of the void is on the downstream side, Fig. 2. The buildup extends to $\sim 0.5\text{--}1\text{ }\mu\text{m}$ upstream of the diamond depression as shown in the height profiles in Fig. 2 and discussed above. It is likely that Te diffuses farther on a step-free plane than on a surface with steps. If facets start to form, they will probably quickly grow by diffusion of the Te atoms to the edges of the facets, where the atoms will then get attached. In this way the faceted surfaces will grow outward and result in the planar surfaces inside the microvoids. If we assume no diffusion from the hole, we can see there will be a “canal” extending from the hole in the $[\bar{1}11]$ direction as there will be no supply of atoms from the hole. There must then be steps in the canal also, so that the preferential Te diffusion moves the atoms that land in the canal to the left and out of the microvoid.

With increasing temperature the microvoids gradually get cut off by an edge parallel to the $[01\bar{1}]$ direction until the diamond has become a triangle with a vertical $(\bar{1}11)$ plane right next to the hole. This could be due to the fact that there is more extra Te available, so that the material buildup goes faster.

C. Mechanism for formation of high-temperature voids

Similar high-temperature voids observed in CdHgTe have been shown to be related to Te precipitation and subsequent polycrystalline growth of CdHgTe. Colin explains the formation of the defects with a Hg deficiency at high growth tem-

perature, whereby Te starts to nucleate and grow, and then polycrystalline CdHgTe starts to form and grows along with the Te.⁸ Aoki *et al.* have performed TEM measurements of the defects and show that they contain polycrystalline material with randomly oriented CdHgTe grains of 30–200 nm.¹¹ The grains are surrounded by crystalline Te, and their EDX measurements show that there is a deficiency of Hg in the voids. Underneath the defect there is single-crystal CdHgTe. Their results support the formation mechanism suggested by Colin. Our EDX measurements are in agreement with those of Aoki *et al.* (Fig. 5). We believe we are looking at the same type of defects in HgTe, and that the onset of high-temperature voids in HgTe also indicates the onset of Te precipitation and gives the Te-phase limit in HgTe. The apparent reduction of polycrystalline material in the high-temperature voids in HgTe layers relative to the CdHgTe layers is probably related to the high binding energy of Cd. This suggests a lower surface mobility for Cd, whereas Hg and Te can either re-evaporate or diffuse further, giving more planar surfaces. The lower growth rate within the defect, leading to the formation of a void in both HgTe and CdHgTe, implies that the incorporation is reduced within the defect. This is not necessarily due to a Hg deficiency alone. It is indeed possible that incorporation on (211)B surfaces is higher than the average incorporation on the randomly oriented polycrystalline surfaces. This is consistent with previous studies comparing incorporation on (211)B and selected other orientations.^{7,17} It is also consistent with the appearance of faceted hillocks rising *above* the films grown on (100) surfaces,²³ indicating that the hillock facets have a higher incorporation rate. Precipitation of excess Te combined with deposition of randomly oriented HgTe (or CdHgTe) therefore accounts for the observation of a Te-rich void-type defect.

D. HgTe HRXRD

The evolution of the 422 HRXRD FWHM with substrate temperature is shown in Fig. 6. For reference, the substrate FWHM was 19 ± 3 arc s. (measured prior to growth). The FWHM of the HgTe epilayer is ~ 40 arc s in the layers grown at and above 189 °C. The 422 FWHM of the best layer is approximately double the substrate FWHM and is most likely due to the misfit between layer and substrate, which is $\sim 10^{-3}$. The FWHM of CdHgTe layers grown on lattice-matched substrates under optimal conditions is ~ 20 arc s.

The increase in FWHM at lower temperatures shows a deterioration of the crystalline quality. A common defect in low-temperature HgTe films is twins. The three layers grown at the lowest substrate temperatures have the largest FWHM and contained 3–15% twins.

A comparison of the surface morphology with the x-ray diffraction data shows that, even when the layer contains a high density of high-temperature voids, the FWHM of the 422 reflections does not indicate a deterioration in crystalline quality. This shows that the material between the defects is high-quality material and that x-ray diffraction is not suffi-

TABLE I. Thermodynamic data (Ref. 22).

Parameter	Value
ΔH_{HgTe}^0	174 312 J/mol
ΔH_{Te}^0	72 693 J/mol
ΔS_{HgTe}^0	178.6 J/(mol K)
ΔS_{Te}^0	65.73 J/(mol K)

cient to screen the HgTe layers. Hence, the surface morphology gives a much better indication of the growth conditions and material quality than the HRXRD FWHM.

E. Thermodynamic modeling of the onset of Te precipitation

A thermodynamic model for MBE growth of CdHgTe was formulated by Gaillard²⁴ and based on the assumption that re-evaporating fluxes obey the mass action law regardless of incident fluxes. Colin⁸ argued that high-temperature voids are consistent with the model's prediction of Te precipitation at growth temperatures above the Te-rich phase limit of CdHgTe. Colin and Skauli⁷ found that the observed optimal growth temperature coincides with model predictions of the Te-rich phase limit for CdHgTe, within experimental uncertainties. Furthermore, they found that this optimal temperature is practically independent of growth rate, in agreement with predictions. Generally, these findings are strong indications that MBE growth of CdHgTe takes place close to thermodynamic equilibrium, and they show that the model's predictions may be of practical interest. Here, we will show that the high-temperature defect behavior of HgTe is consistent with that of CdHgTe and, crucially, that the growth temperature at the onset of high-temperature voids in HgTe can be used to predict the onset of these defects in CdHgTe over a wide range of compositions.

From the thermodynamic model we obtain the following equation for the growth temperature corresponding to the Te-rich phase limit of CdHgTe:

$$T_s = \frac{\Delta H_{\text{HgTe}}^0 - \Delta H_{\text{Te}}^0}{\Delta S_{\text{HgTe}}^0 - \Delta S_{\text{Te}}^0 - R \ln \frac{F_{\text{Hg}} \cdot \alpha_{\text{Hg}}^c \cdot (2\pi m_{\text{Hg}} k T_s)^{1/2}}{\alpha_{\text{Hg}}^v \cdot p_1 \text{ atm}} + R \ln(1-x)}, \quad (1)$$

where ΔH_x^0 and ΔS_x^0 are the enthalpies and entropies of sublimation (see Table I), F_{Hg} is the Hg flux on the substrate, α_{Hg}^c is the Hg condensation coefficient, α_{Hg}^v is the evaporation coefficient, R is the gas constant [8.31 J/(mol K)], $p_1 \text{ atm}$ is the pressure of one atmosphere (101 325 Pa), x is the fractional Cd content in the growing film, and m_{Hg} is the atomic mass of mercury. (This is an implicit expression, with the denominator having a weak dependence on T_s , but by simple iteration a numerical solution is easily found.)

The uncertainties in the values of α_{Hg}^c , α_{Hg}^v , and F_{Hg} are too large to obtain sufficiently accurate predictions of T_s without any fitting to experimental data. However, these parameters enter in the form of a fraction $F_{\text{Hg}} \cdot \alpha_{\text{Hg}}^c / \alpha_{\text{Hg}}^v$, and we

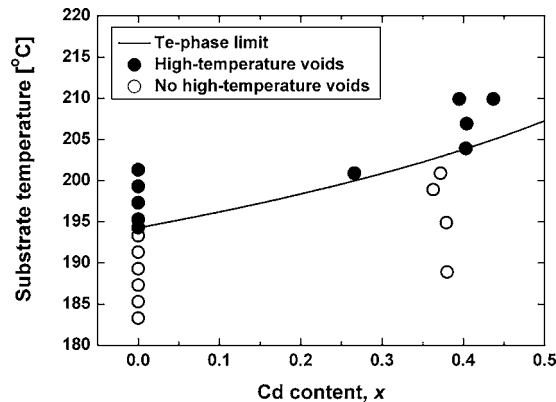


FIG. 8. Plot of the Te-phase limit in $\text{Cd}_x\text{Hg}_{1-x}\text{Te}$ based on a thermodynamic model [Eq. (1)] along with experimental data. Filled circles represent layers containing high-temperature voids, whereas open circles represent layers without high-temperature voids.

are therefore essentially left with only one fitting parameter. $F_{\text{Hg}} = 8.50 \cdot 10^{20} \text{ m}^{-2} \text{ s}^{-1}$ was based on chamber pressure measurement. We choose, somewhat arbitrarily, to set $\alpha_{\text{Hg}}^c = 1$, and to vary α_{Hg}^v so that T_s for HgTe ($x=0$) fits the experimental Te-phase limit at 194.3 °C. This results in a fitted value of 0.28 for α_{Hg}^v . The effect of varying α_{Hg}^v is predominantly to adjust a temperature offset, i.e., to parallel shift the curve vertically.

In Fig. 8, we plot the composition and growth temperature for the HgTe layers discussed here and for a similar series of CdHgTe layers. For each point, it is indicated whether high-temperature voids are observed. (The defect behavior of CdHgTe samples will be discussed in more detail in a separate paper.) Also plotted is the model's prediction of T_s after fitting to the HgTe data only. We see that a good prediction of the Te-phase limit in CdHgTe is obtained. The data on CdHgTe samples shown in Fig. 8 are from samples that were grown immediately after the series of HgTe layers, with the same Hg flux and growth rate. These data are concentrated around $x=0.4$, but our general growth experience is consistent with the predicted curve over the range of compositions up to at least $x=0.5$.

Thus, when the onset of precipitation in HgTe is known, the Te-phase limit for CdHgTe is effectively determined as well. Combined with the fact that we can use the shape of the microvoids in HgTe to determine the deviation from the Te-phase limit, it is clear that by growing one layer of HgTe it is possible to deduce a good estimate of the optimal growth temperature for a given composition of CdHgTe. Thus, in essence we have shown that growth of HgTe can be used as an *in situ* thermometer suitable for establishing and maintaining the highly critical substrate temperature calibration.

IV. SUMMARY

We have mapped the effect of substrate temperature on HgTe growth quality through surface morphology and XRD in a wide temperature interval around the optimal growth temperature. Twins appear at the lowest substrate temperatures, whereas at higher temperatures the crystallinity as ob-

served by XRD is very good, even when the layer contains a high density of high-temperature voids. The high-temperature voids appear at the Te-phase limit and display a slight increase in number density, but a large increase in width, as the temperature increases. Circular voids and hill-ocks are found in samples grown at substrate temperatures $T_{\text{opt}} - 2$ and above.

Microvoids are found at all temperatures. The microvoids are faceted, and their shape depends on the growth temperature. The overall trend as the growth temperature is varied from low to high is that the microvoids develop from diamond-shaped to triangular, and from clusters to single voids. The deviation from optimal substrate temperature in a given layer can thereby be estimated by studying the shape of the microvoids. The number density of the microvoids decreases with temperature throughout the studied range.

We have presented possible mechanisms for the formation of microvoids and high-temperature voids. Microvoids appear to be nucleated by substrate defects/surface impurities and shaped by surface diffusion effects. As is well established, high-temperature voids are clearly related to precipitation of excess Te.

Defect area show that the optimum substrate temperature for growth of HgTe lies just below the Te-phase limit. Furthermore, we have shown that by fitting the thermodynamic model to the onset of Te precipitation in HgTe, we can accurately predict the onset of Te precipitation, and thereby the optimal growth temperature, in CdHgTe. Thus, growth of one HgTe layer may provide a useful way of calibrating CdHgTe growth temperature.

Finally, we have shown that surface morphology is better suited than XRD to screen layers. In a future publication we will discuss defects in CdHgTe.

ACKNOWLEDGMENT

Laila Trosdahl-Iversen is acknowledged for substrate preparation.

- ¹R. Haakenaasen, H. Steen, T. Lorentzen, L. Trosdahl-Iversen, A. D. van Rhee, and H. Syversen, *J. Electron. Mater.* **31**, 710 (2002).
- ²R. Haakenaasen, H. Steen, E. Selvig, T. Lorentzen, A. D. van Rhee, L. Trosdahl-Iversen, H. Syversen, D. Hall, and N. Gordon, *J. Electron. Mater.* **34**, 922 (2005).
- ³G. L. Hansen, J. L. Schmit, and T. N. Casselman, *J. Appl. Phys.* **53**, 7099 (1982).
- ⁴P. S. Wijewarnasuriya, M. Zandian, D. B. Young, J. Waldrop, D. D. Edwall, W. V. McLevige, D. Lee, and J. Arias, *J. Electron. Mater.* **28**, 649 (1999).
- ⁵J. B. Varesi, A. A. Buell, J. M. Peterson, R. E. Bornfreund, M. F. Vilela, W. A. Radford, and S. M. Johnson, *J. Electron. Mater.* **32**, 661 (2003).
- ⁶T. Colin, D. Minsås, S. Gjøn, R. Sizman, and S. Løvold, *Mater. Res. Soc. Symp. Proc.* **340**, 575 (1994).
- ⁷T. Colin and T. Skauli, *J. Electron. Mater.* **26**, 688 (1997).
- ⁸T. Colin, Ph.D. thesis, Université Joseph Fourier, Grenoble, 1991.
- ⁹L. He, Y. Wu, L. Chen, S. L. Wang, M. F. Yu, Y. M. Qiao, J. R. Yang, Y. J. Li, R. J. Ding, and Q. Y. Zhang, *J. Cryst. Growth* **227–228**, 677 (2001).
- ¹⁰Y. Chang, G. Badano, J. Zhao, C. H. Grein, S. Sivananthan, T. Aoki, and D. J. Smith, *Appl. Phys. Lett.* **83**, 4785 (2003).
- ¹¹T. Aoki, Y. Chang, G. Badano, J. Zhao, C. Grein, S. Sivananthan, and D. J. Smith, *J. Electron. Mater.* **32**, 703 (2003).
- ¹²D. Chandra, F. Aqariden, J. Frazier, S. Gutzler, T. Orent, and H. D. Shih, *J. Electron. Mater.* **29**, 887 (2000).

- ¹³J. M. Arias, M. Zandian, J. Bajaj, J. G. Pasko, L. O. Bubulac, S. H. Shin, and R. E. De Wames, *J. Electron. Mater.* **24**, 521 (1995).
- ¹⁴I. V. Sabinina, A. K. Gutakovsky, Yu. G. Sidorov, and A. V. Latyshev, *J. Cryst. Growth* **274**, 339 (2005).
- ¹⁵E. C. Piquette, M. Zandian, D. D. Edwall, and J. M. Arias, *J. Electron. Mater.* **30**, 627 (2001).
- ¹⁶L. H. Zhang and C. J. Summers, *J. Electron. Mater.* **27**, 634 (1998).
- ¹⁷L. A. Almeida, M. Groenert, J. Markunas, and J. H. Dinan, *J. Electron. Mater.* **35**, 1214 (2006).
- ¹⁸M. Kawano, N. Oda, T. Sasaki, T. Ichihashi, S. Iijima, T. Kanno, and M. Saga, *J. Cryst. Growth* **117**, 171 (1992).
- ¹⁹T. Skauli, T. Colin, and S. Løvold, *J. Vac. Sci. Technol. A* **12**, 274 (1994).
- ²⁰M. Martinka, L. A. Almeida, J. D. Benson, and J. H. Dinan, *J. Electron. Mater.* **30**, 632 (2001).
- ²¹D. Chandra, H. D. Shih, F. Aqariden, R. Dat, S. Gutzler, M. J. Bevan, and T. Orent, *J. Electron. Mater.* **27**, 640 (1998).
- ²²R. Haakenaasen, H. Steen, E. Selvig, T. Lorentzen, A. D. van Rheenen, L. Trosdahl-Iversen, D. Hall, N. Gordon, T. Skauli, and A. H. Vaskinn, *Phys. Scr.* **T126**, 31 (2006).
- ²³A. Million, L. Di Cioccio, J. P. Gaillard, and J. Piaguet, *J. Vac. Sci. Technol. A* **6**, 2813 (1988).
- ²⁴J. P. Gailliard, *Rev. Phys. Appl.* **22**, 457 (1987).